

Study of the kinetics of ethanol pyrolysis and oxidation

M. Bozkurt^a, D. Nativel^b, M. Aghsaei^a, M. Fikri^a, N. Chaumeix^b, C. Schulz^a

^aIVG, University of Duisburg-Essen, Germany

^bICARE, CNRS, Orléans, France

1 Introduction

Ethanol as a sustainable fuel surrogate for internal combustion engines has become more important in the past decades and its importance will further increase in the future because of regulatory requirements [1]. There are several important advantages to replace conventional fuels by ethanol: (i) as a renewable energy source it can help to reduce the dependence on fossil fuels; (ii) due to its oxygen content, it produces less particulates; (iii) its anti-knock properties [2] are beneficial to further increase the compression ratio of IC engines. Although the oxidation of ethanol was studied for more than 50 years, some discrepancies in the description of the kinetics of ethanol still persist, in particular there are inconsistencies toward the kinetics of the main decomposition channels. Li et al. [3] studied ethanol pyrolysis in a flow reactor at 1.7–3.0 bar and 1045–1080 K. Species concentrations have been measured by FTIR and gas chromatography and the rate of the reaction $\text{C}_2\text{H}_5\text{OH} \rightarrow \text{C}_2\text{H}_4 + \text{H}_2\text{O}$ was determined. In addition, multichannel unimolecular decomposition was calculated on the basis of RRKM theory and the rate k_1 was verified. A deviation from the rate adopted from Marinov has been postulated. More recently, Sivaramakrishnan et al. [4] studied the decomposition of ethanol, in particular, H-ARAS was used to determine the rates of the following channels $\text{C}_2\text{H}_5\text{OH} \rightarrow \text{C}_2\text{H}_4 + \text{H}_2\text{O}$ (R1), $\text{C}_2\text{H}_5\text{OH} \rightarrow \text{CH}_3 + \text{CH}_2\text{O} + \text{H}$ (R2) and $\text{C}_2\text{H}_5\text{OH} \rightarrow \text{C}_2\text{H}_4 + \text{OH} + \text{H}$ (R3). The H-atom concentration histories were found to depend on the overall rate $k_{\text{overall}} = k_1 + k_2 + k_3$ at short times and only the branching ratio of $k_2 + k_3 / k_{\text{overall}}$ determines the asymptote at longer times. By difference, the rate of reaction k_1 was determined. The primary objective of the present work is to rigorously check available mechanisms of ethanol pyrolysis and oxidation and to obtain experimental data to investigate the high-temperature chemistry of ethanol from shock-tube and laminar-flame-speed measurements to constrain the model.

2 Experimental

2.1 Shock tube

The experiments were conducted in two different diaphragm-type shock-tube facilities behind the reflected shock between 1047 and 2518 K at 1.06 and 2.07 bar. Multiple species were measured simultaneously during the pyrolysis and oxidation of ethanol with a high-repetition-rate (time resolution: 10 μs) time-of-flight mass spectrometer (TOF-MS). The driver section of the shock tube has a length of 2.5 m and the driven section has a length of 6.3 m with a constant inner diameter of 80 mm. The end-flange contains a conical nozzle with a diameter of 60 μm which connects the shock tube to the TOF-MS. The device is equipped with an electron impact ion source with two-stage ion extraction and a two-stage micro-channel plate (MCP) for ion detection either in linear or in reflectron mode. Details about this facility are given in [5]. Concentration-time histories of OH radicals were measured with differential laser absorption in the ultraviolet range probing the $\text{A}^2\Sigma^+ \leftarrow \text{X}^2\Pi(0,0)$ $\text{R}_1(5)$ transition at $32,606.56 \text{ cm}^{-1}$ with a continuous-wave frequency-doubled (Coherent MBD-200) frequency-stabilized ring dye laser (Coherent CR 699-21) that is pumped by a diode-pumped Nd:YAG laser (Coherent Verdi V10). To increase the sensitivity and reduce the effect of laser intensity fluctuations, the detection system was designed with separate reference and probe beams. Half of the output power was di-

rected into the reference pathway and the other half was passing through the shock tube. Two home-made enclosed and UV-enhanced silicon photodiodes (Hamamatsu S1722-02) were used to monitor the laser intensity. The absorption cross sections of OH were taken from [6].

2.2 Spherical bomb

The flame speed was determined using a spherical stainless-steel bomb made from two concentric spheres. The inner volume of the vessel is 476 mm³. In order to ensure a homogeneous temperature, heated thermal fluid circulates between the inner and outer wall of the sphere. The maximum temperature of 500 K, with a precision of 1 K, is measured via a thermocouple on the side of the inner wall of the vessel. The maximum operating pressure is 50 bar and a piezo-electric pressure transducer (Kistler) is used to monitor the pressure during combustion. The mixture is spark-ignited with two tungsten electrodes supplied by a high voltage generator. A high voltage probe and a current probe are connected to an oscilloscope to measure both U and I signals and therefore calculate the energy delivered by the spark ($E = \int UI dt$). The average energy delivered by the high voltage generator is 1.82 mJ with a standard deviation of 0.48 mJ. The spark triggers pressure, voltage, current, and camera measurements at the same time via the oscilloscope and a TTL generator.

Four spherical quartz windows (100 mm diameter, 50 mm thick) are present on the equatorial plane of the vessel for optical diagnostics. The flame front was visualized via a Z-shape schlieren diagnostics coupled with a high-speed camera. A monochromatic light source is used to illuminate the cell via two lenses (diameters of 75 mm and 20 mm and focal length of 150 mm and 22 mm, respectively) and two concave mirrors (diameters 250 mm, focal length 1 m). Two high speed cameras (PHANTOM V711 & V1210) are used to acquire the images. The acquisition rate and resolution varied according to the camera: with V1210 it is set to 21665 fps and 768×768 pixels and with V711 it was 18003 fps and 608×600 pixels. The mixtures were prepared directly inside the spherical vessel using 99.9% pure ethanol (SIGMA-ALDRICH) and laboratory dry air (0.20945 O₂ + 0.7812 N₂ + 0.0093 Ar). Partial pressures of ethanol as well as dry air were measured using capacitive manometers (MKS) of two different scales (133 and 1333 mbar). According to the precision of the manometers, the mixtures were obtained with an accuracy of 0.2%. More details can be found in [7].

3 Results and discussion

3.1 Investigation of the thermal decomposition of ethanol based on TOF-MS

A full mass spectrum measured for a shock-heated mixture is illustrated in Figure 1. The main products detected during the thermal decomposition are C₂H₄, H₂O, C₂H₅OH, and C₂H₂. The two peaks at $m/z = 20$ and 22 stem from neon that is used as bath gas. Argon was used as inert reference gas to account for gas dynamics effects that affect the molecular beam during the sampling through the nozzle. All signals are then evaluated relative to the argon signal. Furthermore, additional calibration experiments with a priori known concentrations were performed with shock-heated mixtures at moderate temperature (~900 K) in order to separate the contribution by the ion-impact fragmentation in the mass spectrometer from the effects of the thermal reactions. In contrast to stable species such as CO, CO₂, C₂H₂, C₂H₄, and C₂H₅OH, where intensity calibration is feasible directly, the calibration for H₂O is not straightforward because of the tendency of H₂O to adsorb on surfaces. Hence, methane oxidation was used as benchmark to calibrate the H₂O signal.

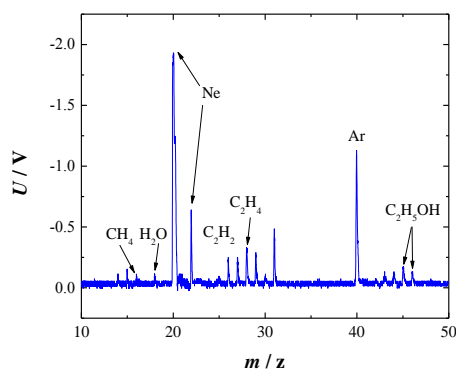


Figure 1: Single mass spectrum for a mixture of 1% C_2H_5OH , 1% Ar and 98.0% Ne at $t = 1500 \mu s$ at $T_5 = 1400 K$ and $p_5 = 1.54$ bar.

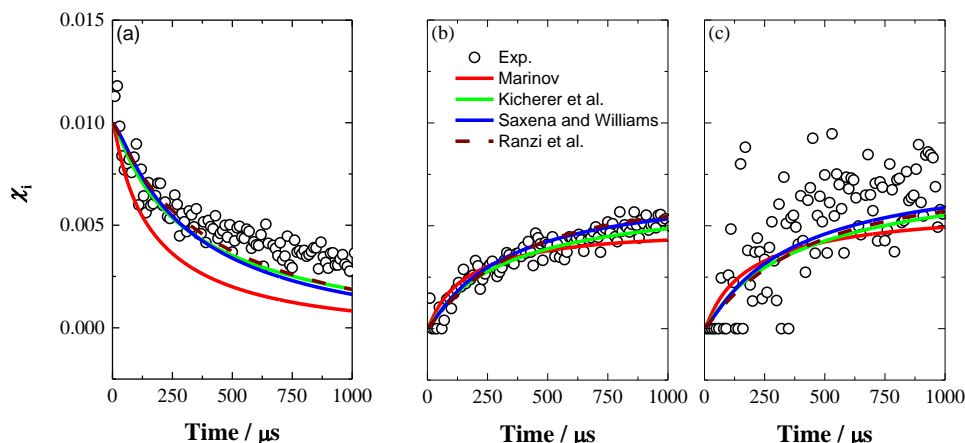


Figure 2: Experimental (symbols) and simulated (lines) of (a) C_2H_5OH , (b) C_2H_4 , and (c) H_2O mole fractions for a shock-heated mixture of 1% C_2H_5OH , 1% Ar and 98.0% Ne at $T_5 = 1400 K$ and $p_5 = 1.54$ bar.

Figure 2 shows experimental and simulated time-resolved concentration profiles of ethanol, ethylene, and water at $T = 1400 K$ and $p = 1.5$ bar. Within 1 ms about 70% of C_2H_5OH is removed. The lines show the results of simulation using the Marinov model [8] (red line) and the model of Saxena and Williams [9] (blue lines), the model of Ranzi (dashed lines) [10] and the model of Kiecherer and co-workers [11] (green lines) where the rates of the main decomposition channels of ethanol were readjusted using statistical rate theory in the Marinov model. Overall, all latter models show a good concordance with the experimental data at short reaction times but deviate at long reaction times, whereas the original Marinov mechanism significantly overpredicts the thermal decomposition of ethanol within the entire temperature range. The carbon balance of the ethanol decomposition reveals that for the specified conditions 30% of the carbon remains in ethanol, around 53% is converted to C_2H_4 and around 17% is present as C_2H_2 (product of C_2H_4). This finding emphasizes the importance of the $CH_3CH_2OH \rightarrow C_2H_4 + H_2O$ channel which is in agreement with the results from [11] at these experimental conditions. While there is good agreement between experimental and simulated data for low temperatures as shown above, all considered mechanisms show large deviations in the concentration-time histories of the corresponding species for temperatures above 1700 K (not shown here). Especially, the simulated ethylene concentration is significantly underestimated when compared with the experimental data.

3.2 Investigation of the oxidation of ethanol based on TOF-MS

Figure 3 shows typical experimental and simulated concentration-time histories of the combustion relevant species H_2O , CO and CO_2 at intermediate temperatures (Figures 3a–c). All mechanisms have in common that the modeling results do not well match the time-resolved experimental observations. Contrary to the results for low temperatures, there is better agreement in the temporal behavior between experiments and simulations for the ethanol oxidation at higher temperatures (cf. Figure 3d–f). The absolute CO concentration at longer reaction times is slightly overpredicted, while the computed CO_2 concentration as a product of carbon monoxide is correspondingly lower. The model of Ranzi et al., however, predicts well these both species.

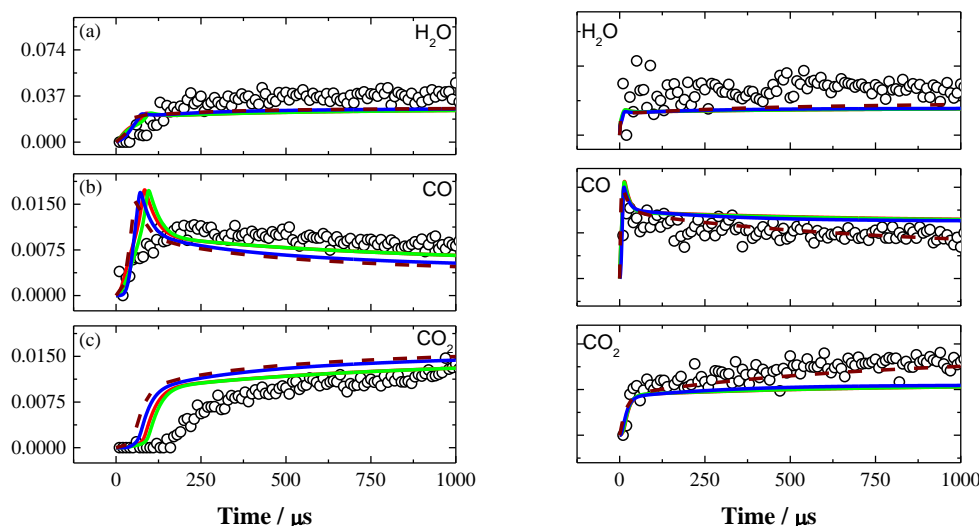


Figure 3: Experimental and simulated profiles for a shock-heated mixture (1% $\text{C}_2\text{H}_5\text{OH}$, 3% O_2 , and 1% Ar balanced with Ne at $T_5 = 1572$ K and $p_5 = 1.40$ bar (left) and at $T_5 = 2222$ K and $p_5 = 1.18$ bar (right).

3.3 Investigation of the oxidation of ethanol based on OH absorption

The temporal variation of OH for a stoichiometric mixture composition at low temperature with its significant two-stage behavior is presented in Figure 4a. The simulations consistently reveal that the first stage is mainly due to the reaction $\text{H} + \text{HO}_2 = 2\text{OH}$ and a minor portion is attributed to $\text{C}_2\text{H}_4\text{OH} = \text{C}_2\text{H}_4 + \text{OH}$, while the second peak shows a strong sensitivity towards the reaction $\text{O}_2 + \text{H} = \text{OH} + \text{O}$. None of the considered reaction mechanisms can reproduce both stages accurately. For higher temperatures the OH-concentration histories show an instantaneous increase without appearance of the first stage. Overall, at low temperature, the best agreement was found with Marinov-based mechanisms, however, the simulated profiles still disagree with the experiments especially at shorter times. The model of Ranzi predicts well the first-stage, deviates however at longer reaction times.

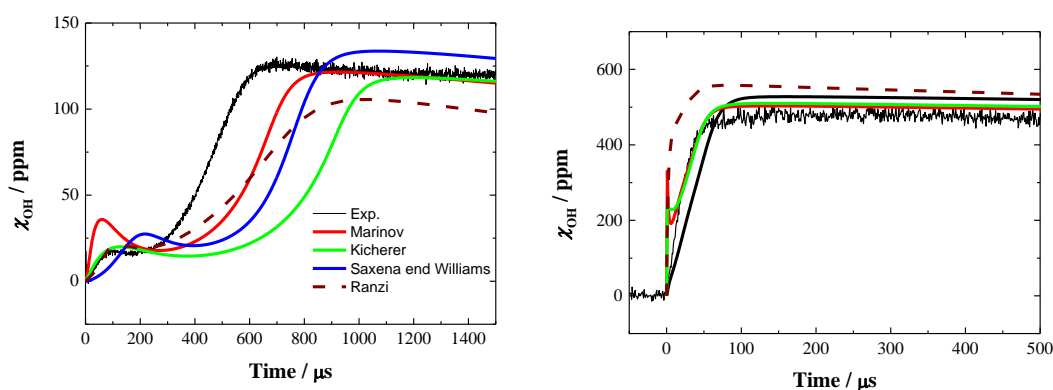


Figure 4: Measured temporal variation of the OH concentration (black lines) for 0.1% C₂H₅OH balanced with argon at (a) $T_5 = 1449$ K and $p_5 = 2.05$ bar and (b) $T_5 = 2293$ K and $p_5 = 1.61$ bar.

3.4 Laminar flame speed

Figure 5a shows a sample of the images recorded during the explosion inside the vessel in the case of a mixture of ethanol with air. For this study, between 100 and 300 images are recorded. Using a home-made code based on Matlab, the flame radius is extracted from each frame to determine the evolution of the radius as a function of time (Figure 5b). The spatial flame speed V_s is deduced from the data, $V_s = dR_f/dt$ with R_f being the flame radius. The observation is limited to the initial stage of the flame expansion where the pressure remains constant, in this case the maximum radius that can be recorded is limited to 48 mm, hence at the maximum radius only about 0.8% of the total volume is being burnt. The evolution of the pressure inside the vessel for this case is reported in Figure 5c the graph zooms on the recording range of images for which the pressure is constant. The simple equation $S_l = \rho_u/\rho_b V_s$ links the spatial flame velocity V_s to the laminar flame speed S_l where ρ_u and ρ_b are the unburned and burned gas density of the mixture, respectively.

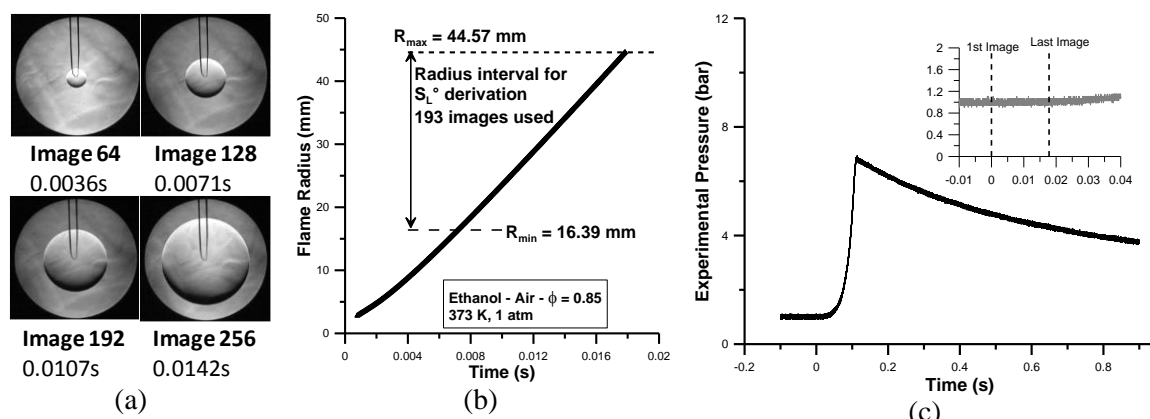


Figure 5: Typical flame images acquired during an explosion and the corresponding radius as a function of time. The mixture, ethanol/air at an equivalence ratio of 0.85, is initially at 1 bar and 373 K.

Due to its spherical geometry the velocity differs from the case of a planar flame. Thus, it is necessary to apply a stretch correction to the velocity either using a linear or a non-linear extrapolation. The unstretched laminar flame speed has been derived for an equivalence ratio ranging from 0.7 to 1.3 at an initial pressure of 1 bar, and from 0.7 to 1.15 at 5 bar. The study at high pressure was limited due to the wrinkling of the flame. Special care has been taken in performing these experiments in order to reduce the experimental error in laminar flame speed determination which is in this case around 1%. As it can be seen in Figure 6a, at 1 bar, the maximum flame speed is 58.5 cm/s for an equivalence ratio around 1.12. When the initial pressure is set to 5 bar, this maximum drops to 39.7 cm/s for the same equivalence ratio. A good agreement is found with the data of Varea et al. [12] at 373 K and 1 bar (Figure 6b) but no data were found at 5 bar for the same initial temperature. At higher temperature of 358 K, one can see that some discrepancies exist in the literature on the rich side.

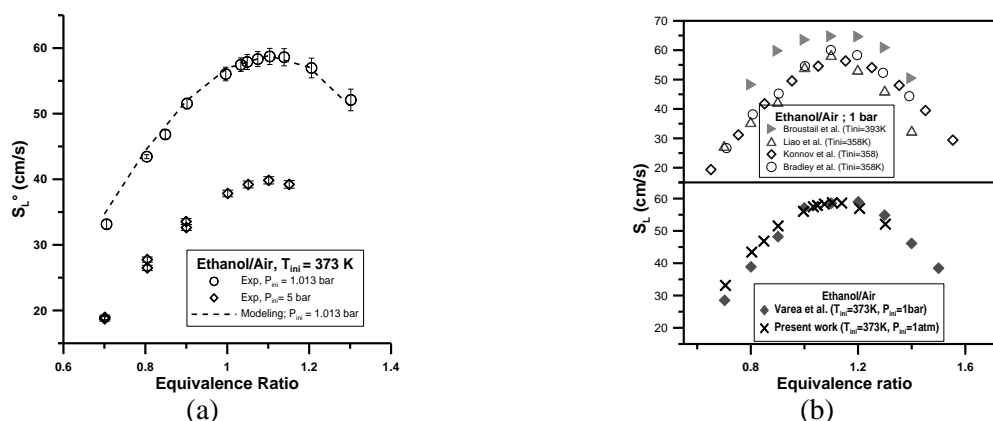


Figure 6: Evolution of the laminar flame speed versus the equivalence ratio for ethanol/air mixtures at two initial pressures, 1 and 5 bar. The initial temperature is 373 ± 0.5 K.

The modeling of the laminar flame of ethanol / air mixtures at an initial pressure of 1.013 bar and temperature of 373 K have been performed using COSILAB software. The detailed kinetic mechanism used for these experiments is the latest of Ranzi et al. [10]. As one can see, an excellent agreement is found between the simulated and the measured values

4 Summary and conclusions

Time-resolved concentration profiles of multiple combustion species such as CO, CO₂, C₂H₂, C₂H₄, and C₂H₅OH were measured for the pyrolysis and the oxidation of ethanol in a shock tube by time-of-flight mass spectrometry. The experiments were conducted behind reflected shock waves between 1047 and 2518 K around atmospheric pressure. Additionally, concentration-time histories of OH were monitored using differential laser absorption at around 306 nm during ethanol oxidation. The mass spectrometry data was compared against simulation results from common ethanol mechanisms from Marinov [8], Saxena and Williams [9] and a modified Marinov mechanism from Kiecherer et al. [11]. Flame-speed measurements were performed for a wide range of conditions. While there is good agreement between experimental and simulation results for the pyrolysis at low temperatures, large discrepancies remains in predicting the temporal occurrence of C₂H₂, C₂H₄, and H₂O for temperatures above 1700 K. For the oxidation and at low temperatures, none of the models can predict the temporal behavior of the respective species especially for short reaction times where the simulation strongly overpredicts CO, CO₂, and H₂O formation. However, their absolute concentration at longer reaction times can be reproduced. For high temperatures, the concordance in terms of temporal behavior as well as absolute concentration of the considered species is fairly good even though notable deviations still persist. OH absorption measurements showed that the Marinov model does a good job at high temperature although its OH prediction is not well at low temperature especially in the build-up of OH. New values of laminar flame speeds, at an initial temperature of 373 K and for 2 initial pressures, were obtained. Special care has been taken in order to reduce the uncertainty in the measurements. The modeling will be undertaken in the very near future.

Acknowledgements

Funding by the German Research Foundation (DFG) and by the French Ministry of Education are gratefully acknowledged.

References

1. in: Directive 2009/28/EC of the European Parliament and of the Council, <http://eur-lex.europa.eu/LexUriServ/LexUriServ.do?uri=L:2009:140:0016:0062:en:PDF>, 2009.
2. H. J. Curran, M. P. Dunphy, J. M. Simmie, C. K. Westbrook, W. J. Pitz, *Proc. Combust. Symp.* 24 (1992) 769-76.
3. J. Li, A. Kazakov, F. L. Dryer, *J. Phys. Chem. A* 108 (2004) 7671-7680.
4. R. Sivaramakrishnan, M. C. Su, J. V. Michael, S. J. Klippenstein, L. B. Harding, B. Ruscic, *J. Phys. Chem. A* 114 (2010) 9425-9439.
5. S. H. Duerrstein, M. Aghsaee, L. Jerig, M. Fikri, C. Schulz, *Rev. Sci. Instrum.* 82 (2011) 084103/1-084103/7.
6. J. T. Herbon, R. K. Hanson, D. M. Golden, C. T. Bowman, *Proc. Combust. Inst.* 29 (2002) 1201-1208.
7. T. Dubois, N. Chaumeix, C.-E. Paillard, *Energy Fuels* 23 (2009) 2453-2466.
8. N. M. Marinov, *Int. J. Chem. Kinet.* 31 (1999) 183-220.
9. P. Saxena, F. A. Williams, *Proc. Combust. Inst.* 31 (2007) 1149-1156.
10. E. Ranzi, A. Frassoldati, R. Grana, A. Cuoci, T. Faravelli, A. P. Kelley, C. K. Law, *Prog. Energy Combust. Sci.* 38 (2012) 468-501
11. J. Kiecherer, T. Bentz, C. Hüllemann, K. Blumenstock, M. Olzmann, in: *5th European Combustion Meeting*, Cardiff, UK, 2011.
12. E. Varea, V. Modica, A. Vandel, B. Renou, *Combust. Flame* 159 (2012) 577-590.
13. G. Broustail, P. Seers, F. Halter, G. Moreac and C. Mounai, *Fuel* 90 (2011) 1-6
14. D. Bradley, M. Lawes, M.S., *Combust. Flame* 156 (2009) 1462-1470
15. A.A. Konnov, R.J. Meuwissen, L.P.H. de Goey, *Proc. Combust. Inst.* 33 (2011) 1011-1019
16. S.Y. Liao, D.M. Jiang, Z.H. Huang, K. Zeng, G. Cheng, *Applied Thermal Engineering* 27(2007) 374-380